

---

# Behavior of Graph Laplacians on Manifolds with Boundary

---

**Xueyuan Zhou**

Department of Computer Science  
University of Chicago  
zhouxy@cs.uchicago.edu

**Mikhail Belkin**

Department of Computer Science and Engineering  
Ohio State University  
mbelkin@cse.ohio-state.edu

## Abstract

In manifold learning, algorithms based on graph Laplacians constructed from data have received considerable attention both in practical applications and theoretical analysis. In particular, the convergence of graph Laplacians obtained from sampled data to certain continuous operators has become an active research topic recently. Most of the existing work has been done under the assumption that the data is sampled from a manifold without boundary or that the functions of interests are evaluated at a point away from the boundary. However, the question of boundary behavior is of considerable practical and theoretical interest. In this paper we provide an analysis of the behavior of graph Laplacians at a point near or on the boundary, discuss their convergence rates and their implications and provide some numerical results. It turns out that while points near the boundary occupy only a small part of the total volume of a manifold, the behavior of graph Laplacian there has different scaling properties from its behavior elsewhere on the manifold, with global effects on the whole manifold, an observation with potentially important implications for the general problem of learning on manifolds.

## 1 Introduction

Graph Laplacian constructed from data points is a key element in many machine learning algorithms including spectral clustering, e.g., (von Luxburg, 2007), semi-supervised learning (Zhu, 2006; Chapelle et al., 2006) and dimensionality reduction (Belkin & Niyogi, 2003), as well as a number of other applications. A large amount of work in recent years has been centered on analyzing various theoretical aspects of graph Laplacians on manifolds, and, in particular, on their different modes of convergence, when the data goes to infinity and/or the parameters, such as kernel bandwidth, tend to zero (Belkin, 2003; Lafon, 2004; Hein, 2005; Coifman & Lafon, 2006; Singer, 2006; Giné & Koltchinskii, 2006; Hein et al., 2007; Belkin & Niyogi, 2008; von Luxburg et al., 2008; Rosasco et al., 2010). A typical result in that direction shows that the discrete graph Laplacian converges<sup>1</sup> to the Laplacian-Beltrami operator on manifolds when the bandwidth parameter of the kernel is chosen as an appropriate function of the number of data points. These results help to clarify our understanding of the underlying objects, to shed light on properties of the algorithms and to guide the selection of algorithms in practical applications.

For example, an analysis of normalized versus unnormalized Laplacians in (von Luxburg et al., 2008) suggests that normalization may be preferable in practical applications. In another example, the estimators of several graph Laplacian based semi-supervised learning algorithms had recently been shown to converge to constant solutions in the limit of infinite unlabeled points while fixing labeled points (Nadler et al., 2009), suggesting the use of iterated Laplacians (Zhou & Belkin, 2011), which indeed shows superior performance in practice.

The spectral convergence of a graph Laplacian is another important limit analysis of the graph Laplacian, which links directly to applications. The empirical spectral convergence of spectral clustering when the sample size  $n$  goes to infinity for a fixed kernel bandwidth  $t$  was studied by (von Luxburg et al., 2008), while the spectral convergence of a graph Laplacian to the Laplace-Beltrami operator when the kernel bandwidth  $t$  goes to zero as  $n$  goes to infinity is studied in (Belkin & Niyogi, 2007).

However, most previous results on graph Laplacians deal with the setting where the manifold does not have a boundary or when the operator is analyzed at a point away from the boundary. Arguably, it is a

---

<sup>1</sup>Different modes of convergence are possible here, such as different types of pointwise or uniform convergence or convergence of eigenvectors.

significant short-coming of these analyses, since manifolds or domains with boundary are present explicitly or implicitly in many problems of significant interest in data analysis. Perhaps the simplest example is the fact that the pixel intensity of a gray-scale image cannot be smaller than zero, providing a natural boundary condition for any image manifolds. A more interesting example is in motion analysis, where the manifold of configurations of a human or robot body (perhaps embedded using video images or data from sensors attached to limbs) has boundaries corresponding to the limits for the range of motions of each individual joint. More generally, it is natural to think that boundaries in data are present whenever the generating process itself is in some way constrained. It is clear that if such manifolds are to be learned from data, the boundary behavior cannot be disregarded.

In the current paper we discuss the boundary behavior of graph Laplacians by analyzing the graph Laplacian convergence at the boundary. We show that the graph Laplacian at the boundary converges to a gradient operator in the direction normal to the boundary, when the bandwidth parameter  $t$  is chosen adaptively as a function of the number of data points. We provide explicit bounds for the convergence. One of the key results of our analysis is that both the behavior and the scaling of the graph Laplacian near the boundary is quite different from that in the interior of the manifold. Specifically, for a fixed function  $f(x)$  and a small bandwidth parameter  $t$  the (appropriately scaled) graph Laplacian will be close to the Laplace-Beltrami operator  $\Delta f(x)$  on interior point  $x$ , while at the boundary the same object will be close to the normal derivative  $\frac{1}{\sqrt{t}}\partial_n f(x)$ . We see that the large values of the graph Laplacian applied to a fixed function are likely to correspond to the boundary points. Moreover, the analysis shows that while there are few points near the boundary of a manifold, their influence on the graph Laplacian is disproportionately large and cannot be ignored. This suggests that the boundary has a global effect on the graph Laplacian, a finding that is confirmed by our numerical experiments provided in the paper. Viewed in a different way it suggests that for algorithms when a graph Laplacian is used as a regularizer, as is the case in many applications, bounding the norm would lead to the suppression of the large values near the boundary. Thus the minimizer of the regularization problem (or similarly, the eigenvectors) should satisfy the Neumann boundary conditions, i.e., be nearly constant in the direction orthogonal to the boundary, which is confirmed by our numerical experiments.

In a related line of investigation we find that the symmetric normalized graph Laplacian  $L^s$  has a different boundary behavior from the random walk (asymmetric normalized) and unnormalized graph Laplacians. Unlike those two, for a fixed function  $f(x)$ ,  $L^s f(x)$  converges to  $\frac{1}{\sqrt{t}}[p(x)]^{1/2}\partial_n(f(x)/[p(x)]^{1/2})$  for a boundary point  $x$ , where  $p(x)$  is the probability density function. This does not lead to the Neumann boundary condition, and seems strange from a practical point of view.

As a further illustration of the importance of boundary conditions in learning theory, we explore the boundary effects for a reproducing kernel in a simple 1-dimensional example. We also discuss the limit of the graph Laplacian regularizer on manifolds with boundary, which cannot be taken for granted to be the same as the limit on  $\mathbb{R}^N$  or manifolds without boundary because of the boundary behavior of graph Laplacians.

Finally we briefly compare the graph Laplacian built from random samples to the Laplacian on regular grids in numerical PDE's.

## 1.1 Problem Setting

We now proceed with a more technical setting of the problem. Let  $\bar{\Omega}$  be a compact Riemannian submanifold of intrinsic dimension  $d$  embedded in  $\mathbb{R}^N$ ,  $\Omega$  the interior of  $\bar{\Omega}$ , and  $\partial\Omega$  the boundary of  $\Omega$ , which we will assume to satisfy the *necessary smoothness conditions*<sup>2</sup>. Given  $n$  random samples  $X = \{X_1, \dots, X_n\}$  drawn i.i.d. from a distribution with a smooth density function  $p(x)$  on  $\bar{\Omega}$  such that  $0 < a \leq p(x) \leq b < \infty$ , we can build a weighted graph  $G(V, E)$  by mapping each sample point  $X_i$  to vertex  $v_i$  and assigning a weight  $w_{ij}$  to edge  $e_{ij}$ . One typical weight function is the Gaussian defined as  $w_{ij} = K_t(X_i, X_j) = 1/t^{d/2}e^{-\|X_i - X_j\|_{\mathbb{R}^N}^2/t}$ , which is used in this paper. Let the  $n \times n$  matrix  $W$  be the edge weight matrix of graph  $G$  with  $W(i, j) = w_{ij}$ , and  $D$  be a diagonal matrix such that  $D_{ii} = \sum_j w_{ij}$ , then the unnormalized graph Laplacian is defined as matrix  $L^u$

$$L^u = D - W \tag{1}$$

There are several ways of normalizing  $L^u$ . For instance, the most commonly used two are the asymmetric random walk normalized version  $L^r = D^{-1}L^u = I - D^{-1}W$  and the symmetric normalized version  $L^s = D^{-1/2}L^u D^{-1/2} = I - D^{-1/2}W D^{-1/2}$ .

Another useful way of building a graph Laplacian is governed by a parameter  $\alpha$  such that we first normalize  $W$  as  $W_\alpha = D^{-\alpha}W D^{-\alpha}$ , then define the unnormalized, random walk and symmetric normalized graph

<sup>2</sup>Instead of spending several pages to describe these smoothness conditions in this paper, we refer readers to (Belkin, 2003; Lafon, 2004; Hein, 2005) for more details.

Laplacians as

$$\begin{aligned} L_\alpha^u &= D_\alpha - W_\alpha \\ L_\alpha^r &= I - D_\alpha^{-1} W_\alpha \\ L_\alpha^s &= I - D_\alpha^{-1/2} W_\alpha D_\alpha^{-1/2} \end{aligned} \quad (2)$$

where  $D_\alpha$  is the corresponding diagonal degree matrix for  $W_\alpha$ . It is easy to see when  $\alpha = 0$ , these graph Laplacians become the commonly used ones without the first step normalization. Therefore, for each value of  $\alpha$ , there are three closely connected empirical graph Laplacians.

The limit study of graph Laplacians primarily involves the limits of two parameters, sample size  $n$  and weight function bandwidth  $t$ . As  $n$  increases, one typically decreases  $t$  to let the graph Laplacian capture progressively a finer local structure.

With a proper rate as a function of  $n$  and  $t$ , the limit of  $L^u f(x)$  for a given smooth function and fixed  $x$  can be shown to be  $\Delta f(x)$  when  $\bar{\Omega}$  is a compact submanifold of  $\mathbb{R}^N$  without boundary and  $p(x)$  is a uniform density. This builds a connection between the discrete graph Laplacian and the continuous Laplace-Beltrami operator  $\Delta$  on manifolds, which in  $\mathbb{R}^d$  can be written as

$$\Delta = \sum_{i=1}^d \frac{\partial^2}{\partial x_i^2} \quad (3)$$

This connection is an important step in providing a theoretical foundation for many graph Laplacian based machine learning algorithms. For instance, harmonic functions used in (Zhu et al., 2003) for semi-supervised learning is in fact a solution of a Laplace equation, with a ‘‘point boundary condition’’ at labeled points.

The limit of  $L_\alpha^r$  and its various aspects, including the finite sample analysis, are studied in (Belkin, 2003; Lafon, 2004; Hein, 2005; Singer, 2006; Giné & Koltchinskii, 2006; Hein et al., 2007; Belkin & Niyogi, 2008; Belkin & Niyogi, 2007). The basic result is that the limit of  $L_\alpha^r f(x)$  for  $x \in \Omega$  is (up to a constant)

$$\frac{1}{t} L_\alpha^r f(x) \xrightarrow{p} -\Delta_s f(x) = -\frac{1}{p^s} \text{div}[p^s \text{grad } f(x)] = -[\Delta + \frac{s}{p} \langle \nabla p(x), \nabla \rangle] f(x) \quad (4)$$

where  $\Delta_s$  is the weighted Laplacian and  $s = 2(1 - \alpha)$ . These papers deal with the analysis of graph Laplacians at an interior point of the manifold and do not deal with boundary behavior. The exception to that is the analysis in (Coifman & Lafon, 2006), which includes manifolds with boundary, assuming the Neumann boundary conditions on the space of functions. Specifically, the Taylor series for the Gaussian convolution in (Coifman & Lafon, 2006, Lemma 9) involves a term containing the normal gradient at the boundary, which can be reformulated to obtain the limit for the graph Laplacian on the manifold boundary. However, there is no explicit discussion of the boundary behavior as well as its implication for learning in (Coifman & Lafon, 2006). Discrete graph Laplacian is not considered in that work. We believe that given the popularity of graph Laplacians in machine learning, the boundary behavior of graph Laplacians deserves a more detailed study.

In Section 2, we state some existing results on the limit analysis of the graph Laplacian as well as some necessary preparatory results, which will be useful for our analysis. Section 3 contains our main Theorem 2, which states that near the boundary, the graph Laplacian converge to the normal gradient and shows the scaling behavior and explicit rates of convergence. We also show how the scaling changes between the boundary and the interior points of the manifold. Numerical examples to support our analyses are provided in Section 4. Several important implications of the boundary behavior of the graph Laplacian are discussed in Section 5.

## 2 Technical Preliminaries

In this section, we review the existing limit analysis of graph Laplacians  $L_\alpha^u$ ,  $L_\alpha^r$  and  $L_\alpha^s$  on points away from the boundary of a compact submanifold. We also provide some technical results useful for our analysis in Section 3.

Given an undirected graph representation of the random sample set  $X$  of size  $n$ , the weight function with parameter  $t$  is defined as

$$w_t(X_i, X_j) = \frac{1}{t^{d/2}} e^{-\frac{\|X_i - X_j\|_{\mathbb{R}^N}^2}{t}} \quad (5)$$

Notice that in this Gaussian weight function, the Euclidean distance should be used, instead of other distance, e.g., the geodesic on manifolds. It is this critical feature that on one hand makes the graph Laplacians computationally attractive, on the other hand has important implications, which will be discussed in the rest this paper.

Define the corresponding discrete degree function as

$$d_{t,n}(X_i) = \frac{1}{n} \sum_{j=1}^n w_t(X_i, X_j) \quad (6)$$

Then we first normalize the weight function to obtain

$$w_{\alpha,t}(X_i, X_j) = \frac{w_t(X_i, X_j)}{[d_{t,n}(X_i)d_{t,n}(X_j)]^\alpha} \quad (7)$$

Note that this weight function also depends on the locations of  $X_i$  and  $X_j$  other than the Euclidean distance  $\|X_i - X_j\|_{\mathbb{R}^N}$ . We use the three subscripts  $\alpha, t, n$  to emphasize the related parameters. The corresponding discrete degree function is

$$d_{\alpha,t,n}(X_i) = \frac{1}{n} \sum_{j=1}^n w_{\alpha,t}(X_i, X_j) = \frac{1}{n} \sum_{j=1}^n \frac{w_t(X_i, X_j)}{[d_{t,n}(X_i)d_{t,n}(X_j)]^\alpha} \quad (8)$$

If the weight matrix for  $w_t(X_i, X_j)$  is  $W_{t,n}$  and the corresponding degree matrix is  $D_{t,n}$ , then the normalized weight matrix is

$$W_{\alpha,t,n} = D_{t,n}^{-\alpha} W_{t,n} D_{t,n}^{-\alpha} \quad (9)$$

By finding the corresponding degree matrix  $D_{\alpha,t,n}$ , the unnormalized graph Laplacian is

$$L_{\alpha,t,n}^u = D_{\alpha,t,n} - W_{\alpha,t,n} \quad (10)$$

and the other two normalized versions are defined accordingly as  $L_{\alpha,t,n}^r = I - D_{\alpha,t,n}^{-1} W_{\alpha,t,n}$  and  $L_{\alpha,t,n}^s = I - D_{\alpha,t,n}^{-1/2} W_{\alpha,t,n} D_{\alpha,t,n}^{-1/2}$ .

For a fixed smooth function  $f(x)$ , and any  $x \in \bar{\Omega}$  (including the samples and unseen points), define  $L_{\alpha,t,n}^u f(x)$  as the following,

$$L_{\alpha,t,n}^u f(x) = \frac{1}{n} \sum_{j=1}^n w_{\alpha,t,n}(x, X_j) (f(x) - f(X_j)) \quad (11)$$

and similarly for the random walk normalized graph Laplacian

$$L_{\alpha,t,n}^r f(x) = \frac{\frac{1}{n} \sum_{j=1}^n w_{\alpha,t,n}(x, X_j) (f(x) - f(X_j))}{d_{\alpha,t,n}(x)} = f(x) - \frac{1}{n} \sum_{j=1}^n \frac{w_{\alpha,t,n}(x, X_j)}{d_{\alpha,t,n}(x)} f(X_j) \quad (12)$$

For  $L_{\alpha,t,n}^s$ , it can be shown that  $L_{\alpha,t,n}^s f(x) = D_{\alpha,t,n}^{-1/2} L_{\alpha,t,n}^u f(x) D_{\alpha,t,n}^{-1/2}$  where  $F(x) = D_{\alpha,t,n}^{-1/2} f(x)$ . Similar notions also apply to the degree functions. The intuition is that we treat vector  $(f(X_1), \dots, f(X_n))^T$  as a sampled continuous function  $f(x)$  on  $\bar{\Omega}$ . As  $n \rightarrow \infty$ , the vector becomes ‘‘closer and closer’’ to  $f(x)$ .

Three useful convergence results for the interior points will be needed in our analysis (Hein et al., 2007):

$$d_{t,n}(x) \xrightarrow{\text{a.s.}} C_1 p(x) \quad (13)$$

where  $C_1 = \int_{\mathbb{R}^d} K(\|u\|^2) du$ , and

$$d_{\alpha,t,n}(x) \xrightarrow{\text{a.s.}} C_1^{1-2\alpha} [p(x)]^{1-2\alpha} \quad (14)$$

The following limit shows that the graph Laplacian on points that are away from the boundary converge to the density weighted Laplace-Beltrami operator with a proper rate of  $n$  and  $t$ .

$$\frac{1}{t} L_{\alpha,t,n}^r f(x) \xrightarrow{\text{a.s.}} -\frac{C_2}{2C_1} \Delta_s f(x) \quad (15)$$

where  $C_2 = \int_{\mathbb{R}^d} K(\|u\|^2) u_1^2 du$ . The limits of  $L_{\alpha,t,n}^u f(x)$  and  $L_{\alpha,t,n}^s f(x)$  can be found in (Hein et al., 2007)

On a  $d$ -dimensional smooth manifold  $\bar{\Omega}$ , for an interior point  $x$ , the small neighborhood around  $x$  is locally equivalent to whole space  $\mathbb{R}^d$ , while for a point on the boundary of  $\bar{\Omega}$ , i.e.  $x \in \partial\Omega$ , the small neighborhood around  $x$  is locally mapped into a *half space* defined as  $\mathbb{R}_+^d = \{x \in \mathbb{R}^d, x_1 \geq 0\}$ . This is a key fact that will be used in this paper.

Next we will need a concentration inequality for the finite sample analysis of the graph Laplacian.

**Lemma 1** (*McDiarmid’s inequality*) Let  $X_1, \dots, X_n, \hat{X}_i$  be i.i.d. random variables of  $\mathbb{R}^N$  from density  $p(x) \in C^\infty(\bar{\Omega})$ ,  $0 < a \leq p(x) \leq b < \infty$ ,  $|f| < M$  and  $f$  satisfies

$$\sup_{X_1, \dots, X_n, \hat{X}_i} |f(X_1, \dots, X_i, \dots, X_n) - f(X_1, \dots, \hat{X}_i, \dots, X_n)| \leq c_i, \quad \text{for } 1 \leq i \leq n \quad (16)$$

then

$$P(|f(X_1, \dots, X_n) - \mathbb{E}[f(X_1, \dots, X_n)]| > \epsilon) \leq 2 \exp\left(-\frac{2\epsilon^2}{\sum_{i=1}^n c_i^2}\right) \quad (17)$$

### 3 Analysis of Graph Laplacian Near Manifold Boundary

In this section, we analyze the limits of the Laplacians  $L_{\alpha,t,n}^r f(x)$ ,  $L_{\alpha,t,n}^u f(x)$  and  $L_{\alpha,t,n}^s f(x)$  when  $x$  is on or near the boundary of manifold  $\bar{\Omega}$ . The argument roughly follows the lines of the convergence arguments in (Belkin, 2003; Hein, 2005; Coifman & Lafon, 2006).

To fix the notation, in the rest of this paper, we use expressions without subscript  $n$  to indicate the corresponding limit as  $n \rightarrow \infty$ , and expressions without subscript  $t$  to for the limits as  $t \rightarrow 0$ .

$$\begin{aligned} w_t(x, y) &= K_t(x, y) = \frac{1}{t^{d/2}} K(x, y) \\ &= \frac{1}{t^{d/2}} K\left(\frac{\|x-y\|_{\mathbb{R}^N}^2}{t}\right) = \frac{1}{t^{d/2}} e^{-\frac{\|x-y\|_{\mathbb{R}^N}^2}{t}} \\ d_t(x) &= \int_{\bar{\Omega}} w_t(x, y) p(y) dy \\ w_{\alpha,t}(x, y) &= \frac{w_t(x, y)}{[d_t(x) d_t(y)]^\alpha} \\ d_{\alpha,t}(x) &= \int_{\bar{\Omega}} \frac{w_t(x, y)}{[d_t(x) d_t(y)]^\alpha} p(y) dy \end{aligned} \quad (18)$$

For smooth  $f(x)$  and  $p(x)$ ,

$$L_{\alpha,t}^u f(x) = \int_{\bar{\Omega}} w_{\alpha,t}(x, y) (f(x) - f(y)) p(y) dy = d_{\alpha,t}(x) L_{\alpha,t}^r f(x) \quad (19)$$

and

$$L_{\alpha,t}^r f(x) = f(x) - \int_{\bar{\Omega}} \frac{w_{\alpha,t}(x, y)}{d_{\alpha,t}(x)} f(y) p(y) dy \quad (20)$$

Similarly,  $L_{\alpha,t}^s f(x)$  can be rewritten as  $L_{\alpha,t}^s f(x) = d_{\alpha,t}^{-1/2}(x) L_{\alpha,t}^u F(x)$  with  $F(x) = d_{\alpha,t}^{-1/2}(x) f(x)$ .

Next we show the limits of the graph Laplacians on boundary point  $x \in \partial\Omega$  as  $t \rightarrow 0$  and  $n \rightarrow \infty$  at a proper rate, when  $\bar{\Omega}$  has a *smooth* boundary.

**Theorem 2** *Let  $f \in C^3(\bar{\Omega})$ ,  $|f(x)| \leq M$ ,  $p(x) \in C^\infty(\bar{\Omega})$ ,  $0 < a \leq p(x) \leq b < \infty$ ,  $\partial\Omega$  be a smooth boundary of  $\Omega$ ,  $x \in \partial\Omega$ , and  $t$  be sufficiently small, then for the unnormalized graph Laplacian  $L_{\alpha,t,n}^u$*

$$P\left(\left|\frac{1}{\sqrt{t}} L_{\alpha,t,n}^u f(x) - \left[-\frac{C_4}{C_3^{2\alpha}} [p(x)]^{1-2\alpha} \partial_{\mathbf{n}} f(x)\right]\right| \geq \epsilon\right) \leq 2 \exp\left(-\frac{nt^{d+1}\epsilon^2}{C_0}\right) \quad (21)$$

for the random walk normalized graph Laplacian  $L_{\alpha,t,n}^r$

$$P\left(\left|\frac{1}{\sqrt{t}} L_{\alpha,t,n}^r f(x) - \left[-\frac{C_4}{C_3} \partial_{\mathbf{n}} f(x)\right]\right| \geq \epsilon\right) \leq 2 \exp\left(-\frac{nt^{d+1}\epsilon^2}{C_0}\right) \quad (22)$$

and for the symmetric normalized graph Laplacian  $L_{\alpha,t,n}^s$

$$P\left(\left|\frac{1}{\sqrt{t}} L_{\alpha,t,n}^s f(x) - \left[-\frac{C_4}{C_3} [p(x)]^{1/2-\alpha} \partial_{\mathbf{n}} \left(\frac{f(x)}{[p(x)]^{1/2-\alpha}}\right)\right]\right| \geq \epsilon\right) \leq 2 \exp\left(-\frac{nt^{d+1}\epsilon^2}{C_0}\right) \quad (23)$$

where  $s = 2(1-\alpha)$ ,  $\mathbf{n}$  is inward normal direction,  $C_0$  only depends on  $M, a, b$  and  $\alpha$ ,  $C_3 = 1/2 \int_{\mathbb{R}^d} K(\|u\|^2) du$ , and  $C_4 = \int_{\mathbb{R}^d} K(\|u\|^2) u_1 du$ .

**Proof:** We first show the limit of the expectation of  $L_{\alpha,t}^u f(x)$  as  $t \rightarrow 0$  in step 1 to 3. Then the limit of  $L_{\alpha,t}^r f(x)$  and  $L_{\alpha,t,n}^s f(x)$  can easily be found with the help of the limit of discrete degree function  $d_{\alpha,t}(x)$ . At last, we obtain the finite sample results by applying Lemma (1).

For a sufficiently small  $t$ , let  $\Omega_1$  be the set of points that are within distance  $O(\sqrt{t})$  from the boundary  $\partial\Omega$  (a thin layer of ‘‘shell’’), and  $\Omega_0 = \bar{\Omega}/\Omega_1$ . We first show that for a small  $t$ ,  $L_{\alpha,t}^u f(x)$  is approximated by two different terms on  $\Omega_0$  and  $\Omega_1$ , and more importantly these two terms have different orders of  $t$ . Then together with the limit of  $d_{\alpha,t}(x)$ , we can find the limit of  $L_{\alpha,t}^r f(x)$  and  $L_{\alpha,t}^s f(x)$ .

Step 1: The key step for the limit analysis of graph Laplacians is the approximation on the manifold. Consider

$$\begin{aligned} L_{\alpha,t}^u f(x) &= \int_{\bar{\Omega}} \frac{K_t(x, y)}{[d_t(x) d_t(y)]^\alpha} (f(x) - f(y)) p(y) dy \\ &= [d_t(x)]^{-\alpha} \int_{\bar{\Omega}} K_t(x, y) [d_t(y)]^{-\alpha} (f(x) - f(y)) p(y) dy \end{aligned} \quad (24)$$

This integral is on the manifold  $\overline{\Omega}$ . In order to study the limit of this integral when  $t \rightarrow 0$ , we can approximate the integral on an unknown smooth manifold by an integral on its tangent space at each point  $x$  when  $t$  is small such that the approximation errors of each step are comparable. For  $x \in \Omega$ , the tangent space is the whole space  $\mathbb{R}^d$ , while for  $x \in \partial\Omega$ , the tangent space is the half space  $\mathbb{R}_+^d$  ( $x_1 \geq 0$ ).

When  $y \in \overline{\Omega}$  is within an Euclidean ball of radius  $O(t^{1/2})$  centered at  $x$ , in the local coordinate around a fixed  $x$ , the origin is point  $x$ , and let  $s = (s_1, \dots, s_d)$  be the local geodesic coordinate of  $y$ ,  $u = (u_1, \dots, u_d)$  be the projection of  $y$  on the tangent space at  $x$ . Then we have the following important approximation (see (Belkin, 2003, Chapter 4.2) and (Coifman & Lafon, 2006, Appendix B)).

$$\begin{aligned} s_i &= u_i + O(t^{3/2}) \\ \|x - y\|_{\mathbb{R}^N}^2 &= \|u\|_{\mathbb{R}^d}^2 + O(t^2) \\ \det\left(\frac{dy}{du}\right) &= 1 + O(t) \end{aligned} \quad (25)$$

Step 2: Now we are ready to approximate each of the five terms in integral (24) when the integral is taken inside a ball centered at  $x$  having radius  $O(t^{1/2})$  in  $\|\cdot\|_{\mathbb{R}^N}$  norm. Notice that  $\|u\|_{\mathbb{R}^d} \sim O(t^{1/2})$ .

$$\begin{aligned} K\left(\frac{\|x-y\|_{\mathbb{R}^N}^2}{t}\right) &= K\left(\frac{\|u\|_{\mathbb{R}^d}^2}{t}\right) + O(t^2) \\ d_t^{-\alpha}(y) &= d_t^{-\alpha}(x) - \alpha d_t^{-\alpha-1}(x) s^T \nabla d_t(x) + O(s^2) \\ &= d_t^{-\alpha}(x) - \alpha d_t^{-\alpha-1}(x) u^T \nabla d_t(x) + O(t) \\ f(x) - f(y) &= -s^T \nabla f(x) - \frac{1}{2} s^T H(x) s + O(s^3) \\ &= -u^T \nabla f(x) - \frac{1}{2} u^T H(x) u + O(t^{3/2}) \\ p(y) &= p(x) + s^T \nabla p(x) + O(s^2) \\ &= p(x) + u^T \nabla p(x) + O(t) \end{aligned} \quad (26)$$

where  $H(x)$  is the Hessian of  $f(x)$  at point  $x$ . Notice that, the order inside of the big oh is determined by the larger one between the approximation error of  $u$  to  $s$  which is  $O(t^{3/2})$ , and the Taylor expansion error on manifold as a function of  $s$ . The other observation is that, the order of the product of these terms is determined by the third term ( $f(x) - f(y)$ ), the highest order of which is  $O(t^{1/2})$ , with the next ones as  $O(t)$  and  $O(t^{3/2})$ . This means it is enough to keep the approximation terms up to order  $t^{1/2}$ .

Combing all the approximation together in a ball of radius  $O(t^{1/2})$  around  $x$ , with a change of variable  $u \rightarrow t^{1/2}u$ , we can obtain  $L_{\alpha,t}^u f(x)$

$$\begin{aligned} L_{\alpha,t}^u f(x) &= \int_{\overline{\Omega}} \frac{K_t(x,y)}{[d_t(x)d_t(y)]^\alpha} (f(x) - f(y)) p(y) dy \\ &= \int_{\overline{\Omega} \cap \mathbb{B}_1(x)} \frac{K_t(x,y)}{[d_t(x)d_t(y)]^\alpha} (f(x) - f(y)) p(y) dy + O(t^{3/2}) \\ &= -\frac{1}{t^{d/2} d_t^\alpha(x)} \int_{\overline{\Omega} \cap \mathbb{B}_2(x)} K(\|u\|_{\mathbb{R}^d}^2) \left[ \left( \frac{1}{d_t^\alpha(x)} - \sqrt{t} \frac{\alpha u^T \nabla d_t(x)}{(d_t(x))^{\alpha+1}} \right) (\sqrt{t} u^T \nabla f(x) + \frac{t}{2} u^T H(x) u) \right. \\ &\quad \left. (p(x) + \sqrt{t} u^T \nabla p(x)) \right] t^{d/2} du + O(t^{3/2}) \\ &= -\frac{1}{d_t^\alpha(x)} \int_{\mathbb{T}(x)} K(\|u\|_{\mathbb{R}^d}^2) \left\{ \sqrt{t} \left[ \frac{p(x)}{d_t^\alpha(x)} (u^T \nabla f(x)) \right] + \right. \\ &\quad \left. t \left[ \frac{u^T \nabla f(x) \times u^T \nabla p(x)}{d_t^\alpha(x)} - \alpha \frac{p(x) u^T \nabla d_t(x) \times u^T \nabla f(x)}{d_t^{\alpha+1}(x)} + \frac{1}{2} \frac{p(x)}{d_t^\alpha(x)} u^T H(x) u \right] \right\} du \\ &\quad + O(t^{3/2}) \end{aligned} \quad (27)$$

where  $\mathbb{B}_1(x)$  is a ball of radius  $O(t^{1/2})$  in  $\|\cdot\|_{\mathbb{R}^N}$  norm centered at  $x$ , while  $\mathbb{B}_2(x)$  is a ball of radius  $O(t^{1/2})$  in  $\|\cdot\|_{\mathbb{R}^d}$  norm, and  $\mathbb{T}(x)$  is the tangent space at point  $x$ . For a sufficiently small  $t$ , the first step replaces the integral over the whole  $\overline{\Omega}$  with ball  $\mathbb{B}_1(x)$ , generating an error  $O(t^{3/2})$  (Coifman & Lafon, 2006, Appendix B). Then this integral is the same as the integral over a ball on the manifold  $\overline{\Omega}$ . Finally, for an interior point  $x$ ,  $\mathbb{T}(x) = \mathbb{R}^d$ , which means function  $K(\|u\|_{\mathbb{R}^d}^2)$  is a even function of  $u$ . When taking the integral, the first term which has order  $\sqrt{t}$  is odd and therefore vanishes. Then the three left terms that are of order  $t$  inside the

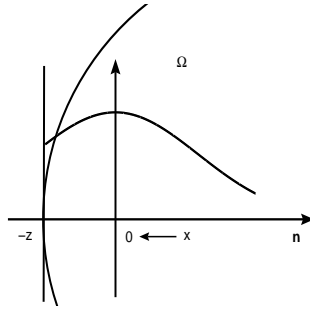


Figure 1: Gaussian weight at  $x$  near the boundary.

integral are exactly the weighted Laplacian at  $x$ , which is of order  $t$ . For a boundary point  $x$ ,  $\mathbb{T}(x) = \mathbb{R}_+^d$ . Next we study the interior points.

Step 3: In Figure. 1,  $x \in \Omega_1$  (the “shell”) is a point near the boundary,  $\mathbf{n}$  is the inward normal direction, and  $-z$  is the nearest boundary point to  $x$  along  $\mathbf{n}$ . In the local coordinate system,  $x$  is the origin, and along the normal direction the Gaussian convolution is from  $-z$  to  $+\infty$ , which is not symmetric. Therefore,  $K(\|u\|_{\mathbb{R}^d}^2)$  is not an even function in the normal direction, so the highest order term is the order  $O(\sqrt{t})$  term.

In this case, all the odd terms of  $u_i$  still will vanish in all directions except the normal direction  $\mathbf{n}$ , and the most important point is that the leading term along the normal direction is of order  $\sqrt{t}$ , while for interior points it is  $t$ . Next we assume  $u_1$  is the normal direction.

$$\frac{1}{\sqrt{t}}L_{\alpha,t}^u f(x) = -\frac{1}{d_t^{2\alpha}(x)}p(x)\partial_{\mathbf{n}}f(x) \int_{-\infty}^{+\infty} \cdots \int_{-\infty}^{+\infty} \int_{-z}^{\infty} K(\|u\|_{\mathbb{R}^d}^2)u_1 du_1 du_2 \cdots du_d + O(\sqrt{t}) \quad (28)$$

where  $z$  is the distance to the nearest point of  $x$  on the boundary  $\partial\Omega$  along the normal direction ( $z \geq 0$ ) as shown in Figure 1. When  $t \rightarrow 0$ ,  $z \rightarrow 0$  in the local coordinate system

$$\lim_{t \rightarrow 0} \frac{1}{\sqrt{t}}L_{\alpha,t}^u f(x) = -\frac{C_4}{C_3^{2\alpha}}[p(x)]^{1-2\alpha} \partial_{\mathbf{n}}f(x) \quad (29)$$

where  $C_3 = \int_{\mathbb{R}_+^d} K(\|u\|^2)du = 1/2C_1$ ,  $C_4 = \int_{\mathbb{R}_+^d} K(\|u\|^2)u_1 du$ . This result also needs the following limits, which generalize (Hein, 2005, Proposition 2.33) to points on the boundary.

$$\lim_{t \rightarrow 0} d_{\alpha,t}(x) = \begin{cases} C_1^{1-2\alpha} p^{1-2\alpha}(x), & \text{for } x \in \Omega \\ C_3^{1-2\alpha} p^{1-2\alpha}(x), & \text{for } x \in \partial\Omega \end{cases} \quad (30)$$

Step 4: The normalized graph Laplacians can be obtained by normalization through  $d_{\alpha,t}(x)$ . Then the limit of the random walk normalized graph Laplacian is (we include the limit for interior point  $x$  for comparison)

$$\lim_{t \rightarrow 0} \frac{1}{t}L_{\alpha,t}^r f(x) = -\frac{C_2}{2C_1} \Delta_s f(x), \text{ for } x \in \Omega \quad (31)$$

$$\lim_{t \rightarrow 0} \frac{1}{\sqrt{t}}L_{\alpha,t}^r f(x) = -\frac{C_4}{C_3} \partial_{\mathbf{n}}f(x), \text{ for } x \in \partial\Omega$$

As for the limit of  $L_{\alpha,t,n}^s$ , it can be shown that  $L_{\alpha,t,n}^s f(x) = D_{\alpha,t,n}^{-1/2} L_{\alpha,t,n}^u F(x)$  where  $F(x) = D_{\alpha,t,n}^{-1/2} f(x)$ . Then the limit analysis follows easily.

Step 5: Consider

$$\frac{1}{\sqrt{t}}L_{\alpha,t,n}^u f(x) = \frac{1}{n\sqrt{t}} \sum_{i=1}^n K_t(x, X_i) [d_{\alpha,t,n}(x) d_{\alpha,t,n}(X_i)]^{-\alpha} [f(x) - f(X_i)] \quad (32)$$

Notice that in the sum, different terms are not independent, since the degree  $d_{\alpha,t,n}(x)$  and  $d_{\alpha,t,n}(X_i)$  includes sums of all the random variables. Therefore, we need to use the McDiarmid’s inequality in this step. The maximum change if we change a random variable is bounded by

$$\frac{1}{nt^{(d+1)/2}} \cdot \frac{1}{a^{2\alpha}} \cdot 2M \quad (33)$$

The maximum change happens when we move a point  $X_i$  from a high density region with a minimum function value to a point  $\hat{X}_i$  in a low density region with a maximum function value. Similar analyses apply

to normalized graph Laplacians. Then We conclude the proof by applying the McDiarmid’s inequality.  $\blacksquare$

Notice that the error rate essentially comes from the McDiarmid’s inequality. When  $\alpha = 0$ , all terms in equation (32) are i.i.d., then we can use the Bernstein’s inequality to obtain a better rate for  $L^u$ . For  $L^r$ , an even better rate can be obtained as shown by (Singer, 2006). When  $\alpha \neq 0$ , although strictly speaking the terms in equation (32) are not i.i.d., since  $d_{\alpha,t,n}(x)$  is really an average of all the samples, it is almost a function of  $x$  alone, and  $d_{\alpha,t,n}(X_i)$  a function of  $X_i$  alone. Then in this case, we believe it is possible to obtain a better error rate.

Together with the existing analysis for interior points, we have the following implication of Theorem (2)

$$\begin{aligned} \frac{1}{t}L_{\alpha,t,n}^r f(x) &\approx -\frac{C_2}{2C_1}\Delta_s f(x), \text{ for } x \in \Omega \\ \frac{1}{\sqrt{t}}L_{\alpha,t,n}^r f(x) &\approx -\frac{C_4}{C_3}\partial_{\mathbf{n}} f(x), \text{ for } x \in \partial\Omega \end{aligned} \quad (34)$$

Therefore, the graph Laplacian converges to a different limit on  $x \in \partial\Omega$  from that on  $x \in \Omega$ . More importantly, these two limits are of different orders, one is  $O(t)$  while the other is  $O(\sqrt{t})$ . However, in practice, when we apply the normalization step, we do not know where the boundary is, and always apply a *global* normalization  $\frac{1}{t}$  for all  $x \in \bar{\Omega}$  in order to obtain the weighted Laplacian in the limit. For a small  $t$

$$\frac{1}{t}L_{\alpha,t}^r f(x) = \begin{cases} -\frac{C_2}{2C_1}\Delta_s f(x) + O(t^{1/2}), & \text{for } x \in \Omega_0 \\ -\frac{C_4}{C_3}\frac{1}{\sqrt{t}}\partial_{\mathbf{n}} f(x) + O(1), & \text{for } x \in \Omega_1 \end{cases} \quad (35)$$

Notice that the  $O(1)$  error only happens on a “shell”  $\Omega_1$  having volume  $O(\sqrt{t})$ . For  $f(x)$  such that  $\partial_{\mathbf{n}} f(x) \neq 0$  on the boundary point  $x$  with enough data points, we have that for small values of  $t$

$$\frac{1}{t}L_{\alpha,t}^r f(x) = O\left(\frac{1}{\sqrt{t}}\right) \quad (36)$$

## 4 Numerical Examples

In this section, we explore the boundary behavior of the graph Laplacian by studying numerical examples.

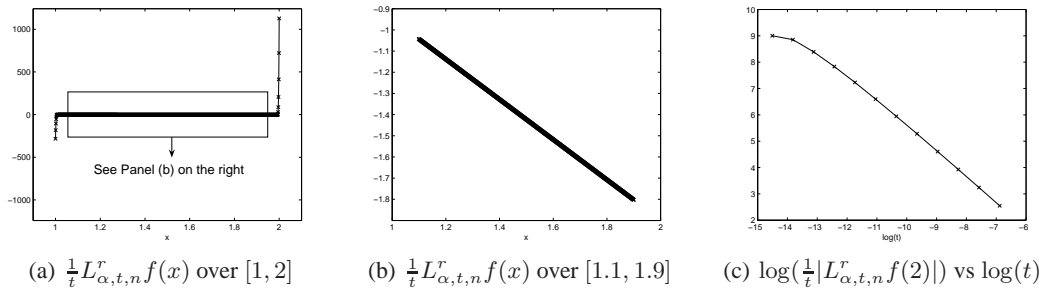


Figure 2:  $\frac{1}{t}L_{\alpha,t,n}^r f(x)$  with  $f(x) = x^3$  over  $[1, 2]$ .

### 4.1 Graph Laplacian on the Boundary

**Example 1.** We take  $\bar{\Omega} = [1, 2]$ , and  $f(x) = x^3$ . The values of  $\frac{1}{t}L_{\alpha,t,n}^r f(x)$  with  $\alpha = 0$  for 1000 points sampled from a uniform distribution (equal-spaced points) and  $t = 10^{-5}$  are shown in Panel (a) in Figure (2). As expected, we see that the values at the boundary are much larger than those inside the domain and are consistent with  $-(x^3)' = -3x^2$  (the value at 2 is roughly 4-times of the value at 1) up to a scaling factor<sup>3</sup>.

In Panel (b) we show the interior  $[1.1, 1.9]$  of the interval where the function is indeed the Laplacian  $-(x^3)'' = -6x$  up to a scaling factor. In Panel (c) we analyze the scaling of the graph Laplacian on the boundary as a function of  $t$  in the log-log coordinates. We see that  $\log \frac{1}{t}|L_{\alpha,t,n}^r f(2)|$  is close to a linear function of  $\log(t)$  with slope approximately  $-\frac{1}{2}$  as you would expect from the scaling factor  $\frac{1}{\sqrt{t}}$ .

<sup>3</sup>The positive value at  $x = 2$  is the result of the normal direction pointing inward (left).

**Example 2.** Next we analyze the boundary behavior for a simple low dimensional manifold. Let  $\overline{\Omega}$  be half a unit sphere ( $z \geq 0$ ), which is a 2-dimensional submanifold in  $\mathbb{R}^3$ . The boundary is a unit circle  $\{(x, y, z) : (x^2 + y^2 = 1, z = 0)\}$ . We take  $f(x, y, z) = xz$ , then the negative inward normal gradient on the boundary is

$$-\partial_{\mathbf{n}}f(x) = -(z, 0, x)(0, 0, 1)^T = -x \quad (37)$$

where  $(z, 0, x)$  is the gradient of  $f(x, y, z)$ , and  $(0, 0, 1)$  is the inward normal direction. This means the negative normal gradient of  $f$  along the inward normal direction on the boundary of a half sphere is a linear function in  $x$  with a negative slope.

We generate a uniform sample set of 2000 points on a half sphere and compute a vector  $g = \frac{1}{\sqrt{t}}L_{\alpha,t,n}^r f(X)$  with  $\alpha = 0, t = 0.5$ . We pick the set  $B = \{(x, y, z) \in X | 0 \leq z \leq 0.05\}$  to be points near the boundary. The dependence between  $\frac{1}{\sqrt{t}}L_{\alpha,t,n}^r f(x, y, z)$  and  $x$  for 2000 data points sampled from the uniform distribution on the half sphere is plotted in Figure (3) and is consistent with our expectation.

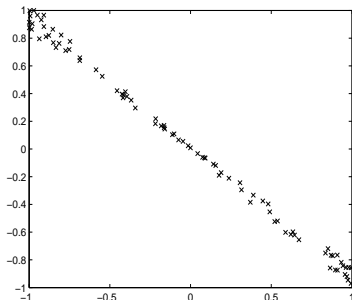


Figure 3:  $\frac{1}{\sqrt{t}}L_{\alpha,t,n}^r f(x)$  on the boundary of a uniform half sphere, with  $t = 0.5$ .

To provide a more rigorous error analysis we compute the mean square errors for several values of  $t$  and sample size  $n$ . The results are shown in Table (1). We see that the errors are relatively small compared to the values of the gradient and generally decrease with more data.

Table 1: Mean square errors between the analytical normal gradient  $-\partial_{\mathbf{n}}f(x, y, z) = -x$  and  $\frac{1}{\sqrt{t}}L_{\alpha,t,n}^r f(x, y, z)$  on the boundary of a half sphere with  $f(x, y, z) = xz$ .

$n \setminus t$	64/64	32/64	16/64	8/64	4/64	2/64	1/64
500	0.0090	0.0059	0.0071	0.0136	0.0287	0.0500	0.0725
1000	0.0089	0.0048	0.0033	0.0061	0.0121	0.0294	0.0627
2000	0.0113	0.0076	0.0073	0.0068	0.0159	0.0356	0.0585
4000	0.0083	0.0044	0.0036	0.0044	0.0072	0.0189	0.0516

## 4.2 Comparison to Numerical PDE's

From previous analysis we can see that, for graph Laplacians, the “missing” edges going out of the manifold boundary on one hand can be seen as being reflected back into  $\overline{\Omega}$ , which is particularly intuitive in symmetric  $k$ NN graphs, see e.g., (Maier et al., 2009), on the other hand, it can be seen that function values on edges going out of  $\overline{\Omega}$  are constant along the normal direction. The latter view is commonly used in schemes of numerical PDE's in finite difference methods for the Neumann boundary condition, see e.g., (Allaire, 2007).

We use an example in  $\mathbb{R}^2$  to show how the Neumann boundary condition for a Laplace operator on a regular grid is implemented in finite difference method, which we hope can shed light on the graph Laplacian on random points. The Laplace operator in  $\mathbb{R}^2$  is  $\Delta f = -\partial_x^2 f - \partial_y^2 f$ , and the regular grid near the boundary is shown in Figure (4). Since we can separate the Laplacian into partial derivatives of different dimensions, the discrete Laplace matrix  $L$  on the regular grid with the Neumann boundary condition near  $x_0$  along  $x$  direction can be shown to be

$$L = \begin{matrix} x_0 \\ x_1 \\ x_2 \end{matrix} \begin{bmatrix} 1 & -1 & 0 & 0 & 0 & \dots \\ -1 & 2 & -1 & 0 & 0 & \dots \\ 0 & -1 & 2 & -1 & 0 & \dots \end{bmatrix}$$

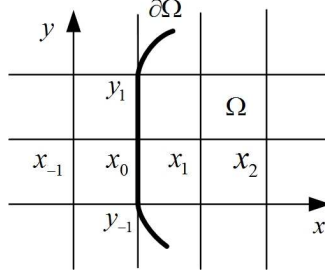


Figure 4: Regular grid in  $\mathbb{R}^2$ .

where we only connects points that are next to each other. Along  $y$  direction the Laplace matrix elements near  $x_0$  are  $[\dots -1 \ 2 \ -1 \ \dots]$ . Let the distance between data points be  $h$ . Consider point  $x_0$  on the boundary, along  $y$  direction, we have a 3-point stencil along  $y$  axis,  $y_{-1}, y_0 = x_0, y_1$ , which is enough to define  $\partial_y^2 f(x_0)$ .

$$\lim_{h \rightarrow 0} \frac{1}{h^2} Lf(y_0) = - \lim_{h \rightarrow 0} \frac{f(y_{-1}) - 2f(y_0) + f(y_1)}{h^2} = -\partial_y^2 f(y_0)$$

This is also true for points that are in the interior  $\Omega$ , e.g.  $x_1, x_2$ , etc. However, for  $x_0$  on the boundary along  $x$  direction (normal direction at  $x_0$ ) we only have two points

$$\lim_{h \rightarrow 0} \frac{1}{h^2} Lf(x_0) = - \lim_{h \rightarrow 0} \frac{f(x_1) - f(x_0)}{h^2} \rightarrow - \lim_{h \rightarrow 0} \frac{\partial_x f(x_0)}{h}$$

This shows that  $Lf(x)$  “converge” to  $\frac{1}{h} \partial_{\mathbf{n}} f(x)$  for  $x$  on the boundary while to  $\Delta f(x)$  for  $x$  inside of the domain, with a different scaling behavior. This is almost the same as what happens to the graph Laplacian on random samples. Notice in numerical PDE’s we also have that if  $\partial_x f(x_0) \neq 0$ , as  $h \rightarrow 0$ ,  $\frac{\partial_{\mathbf{n}} f(x_0)}{h} \rightarrow \infty$ . In fact, if we construct the graph Laplacian matrix  $D - W$  by setting  $w_{ij} = 1$  if two points are next to each other and  $w_{ij} = 0$  otherwise, on two dimensional grid as shown in Figure (4), the graph Laplacian matrix is the same as the Laplace matrix with the *Neumann boundary condition* in numerical PDE’s.

In order to let  $Lf(x)$  converges to  $\Delta f(x)$  for all  $x$  on domain  $\bar{\Omega}$  with a single normalization term, we can add a ‘fictitious’ point  $x_{-1}$  along the normal direction, and let  $f(x_{-1}) = f(x_0)$ . Then as  $h \rightarrow 0$  we have

$$\frac{1}{h^2} Lf(x_0) = - \frac{f(x_1) - f(x_0)}{h^2} = - \frac{f(x_{-1}) - 2f(x_0) + f(x_1)}{h^2} \rightarrow -\partial_x^2 f(x_0)$$

Together with  $y$  direction, we have  $\forall x \in \bar{\Omega}$ ,  $\lim_{h \rightarrow 0} Lf(x) = -\partial_x^2 f(x) - \partial_y^2 f(x) = \Delta f(x)$ . Condition  $f(x_{-1}) = f(x_0)$  then becomes

$$\lim_{h \rightarrow 0} \frac{f(x_{-1}) - f(x_0)}{h} = \partial_x f(x_0) = 0$$

which is the Neumann boundary condition. This method is used to implement the Neumann boundary condition in finite difference methods for PDE’s, see e.g., (Allaire, 2007, Chapter 2).

The graph Laplacian can be seen as an implementation of the Neumann Laplacian on random points, which generalizes regular grids to random graphs based on random samples. This also means by construction, the graph Laplacian is a *Neumann Laplacian*, which is a built-in feature of the graph Laplacian.

## 5 Discussions and Implications

### 5.1 Neumann Boundary Condition

Our analysis of the boundary behavior suggests that the eigenfunctions of both  $L_\alpha^r$  and  $L_\alpha^u$  as well as solutions of certain regularization problems should satisfy the Neumann boundary condition. However, this is not true for the symmetric normalized Laplacian  $L_\alpha^s$ .

**Unnormalized and Random Walk Normalized Graph Laplacians:** These two versions of graph Laplacians only differ in the density weight outside of the normal gradient, so we only need to find the boundary condition for one of them. Let  $\phi_i(x)$  and  $\lambda_i$  be the  $i^{th}$  right eigenfunctions of  $L_\alpha^r$ , then for any positive integer  $i$  and  $x \in \partial\Omega$ , the following Neumann boundary condition holds.

$$\partial_{\mathbf{n}} \phi_i(x) = 0 \tag{38}$$

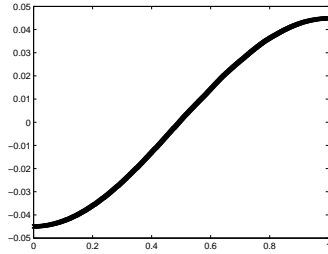
This is also true for the eigenfunctions of  $L_\alpha^u$ , the limit of the unnormalized graph Laplacian, which can be seen as follows. All the eigenfunctions should satisfy

$$\lim_{t \rightarrow 0} \frac{1}{t} L_{\alpha,t}^r \phi_i(x) = L_\alpha^r \phi_i(x) = \lambda_i \phi_i(x)$$

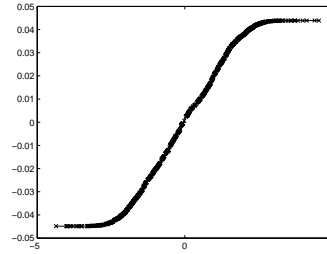
On the boundary

$$\lim_{t \rightarrow 0} \frac{1}{t} L_{\alpha,t}^r \phi_i(x) = - \lim_{t \rightarrow 0} \frac{1}{\sqrt{t}} \partial_{\mathbf{n}} \phi_i(x)$$

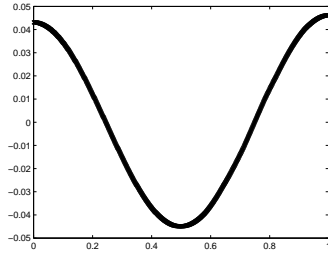
Since  $\lambda_i \phi_i(x) < \infty$  for all  $x \in \overline{\Omega}$ , if  $\phi_i(x)$  does not satisfy the Neumann boundary condition, then  $\lim_{t \rightarrow 0} \frac{1}{t} L_{\alpha,t}^r \phi_i(x) \rightarrow \infty$  on the boundary, therefore such  $\phi_i(x)$  can not be the eigenfunctions of  $L_\alpha^r$ . This implies that all the eigenfunctions of  $L_\alpha^r$  should satisfy the Neumann boundary condition, i.e.,  $\forall i, \partial_{\mathbf{n}} \phi_i(x) = 0$  for  $x \in \partial\Omega$ . Similarly, this is true for the unnormalized graph Laplacian with a bounded density.



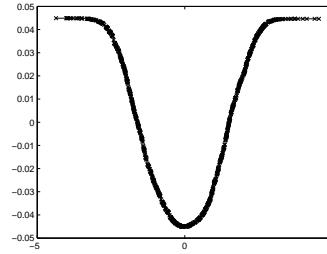
(a)  $\phi_2(x)$  for uniform over unit interval.



(b)  $\phi_2(x)$  for mixture of two Gaussians.



(c)  $\phi_3(x)$  for uniform over unit interval.



(d)  $\phi_3(x)$  for mixture of two Gaussians.

Figure 5: The eigenfunctions of the graph Laplacian for a uniform density and a mixture of two Gaussians centered at  $\pm 1.5$  with unit variance in  $\mathbb{R}^1$ .

We numerically compute the second and third eigenfunctions of  $L_{\alpha,t,n}^r$  with  $\alpha = 1/2$  in Figure (5)<sup>4</sup>. The left panel shows the eigenfunctions over interval  $[0, 1]$  with a uniform density, while the right panel is for a mixture of two Gaussians. As the numerical results suggest, the second and third eigenfunctions of the graph Laplacian satisfy the Neumann boundary condition, and this is also true for other eigenfunctions. In fact for a uniform over  $[0, 1]$ , the Neumann eigenfunctions for the Laplacian are  $\cos(k\pi x)$  where  $k = 0, 1, 2, \dots$ . The second and third eigenfunctions correspond to  $\cos(\pi x)$  and  $\cos(2\pi x)$ , up to a change of sign, which is consistent with the numerical results in the left panel of Figure (5).

**Symmetric Normalized Graph Laplacian:** For the symmetric normalized graph Laplacian  $L_{\alpha,t,n}^s$ , the Neumann boundary condition does not hold for its eigenfunctions in the limit. This can be shown by a one to one correspondence between the eigenfunctions of  $L_{\alpha,t,n}^s$  and  $L_{\alpha,t,n}^r$ . Let the eigenvectors for  $L_{\alpha,t,n}^s$  be  $\psi_i$ , and the right eigenvectors for  $L_{\alpha,t,n}^r$  be  $\phi_i$ , then

$$\psi_i(X_i) = d^{1/2}(X_i) \phi_i(X_i)$$

This is true for any sample size and any parameter  $t$ . Therefore, in the limit

$$\partial_{\mathbf{n}} \psi_i(x) = \partial_{\mathbf{n}} [d^{1/2}(x) \phi_i(x)] = \phi_i(x) \partial_{\mathbf{n}} d^{1/2}(x)$$

<sup>4</sup>The Neumann boundary condition also holds for other  $\alpha$ .

Near the boundary along the normal direction, degree function  $d(x)$  decreases as a result of the asymmetric interval for  $\int_{\bar{\Omega}} K_t(x, y)p(y)dy$ , so  $\psi_i(x)$  tends to be “bent” towards zero near the boundary. Since how the graph is constructed will determine what the degree function will be, the boundary behavior also depends on what graph is used. We test two graphs,  $\epsilon$ NN graph and symmetric  $k$ NN graph, which are studied by (Maier et al., 2009) for clustering. In the left panel of Figure (6),  $d(x)$  is scaled and shifted to fit the plot and an  $\epsilon$ NN graph is used. For  $x$  near the boundary, the degree function decreases as a result of having less points in the fixed radius neighborhood. Therefore,  $\psi_2(x)$  is “bent” towards zero.

Notice that for the symmetric  $k$ NN graph, in the right panel of Figure (6), the eigenfunctions can have “bumps” near the boundary. This is the result that for symmetric  $k$ NN graphs, the edges going out of the boundaries are “reflected” back. For example consider  $k = 10$  in a symmetric  $k$ NN graph, with the distance between points set as 0.01, for point  $x = 0$ , its nearest neighbors are  $x = 0.01, 0.02, \dots, 0.1$ . However, for point  $x = 0.1$ ,  $x = 0$  is not in its  $k$  nearest neighbors. This means the constructed graph will not be symmetric. If we add  $e_{ji}$  for every asymmetric edge  $e_{ij}$ , then although the graph is symmetric now,  $d(x)$  for point  $x = 0.1$  will be much larger than other points. As  $t$  decreases, this “bumps” will shift to the boundary.

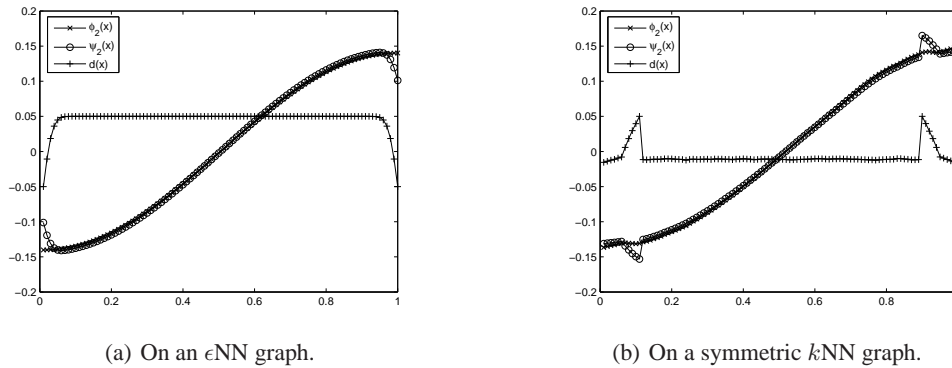


Figure 6:  $\psi_2(x)$ ,  $\phi_2(x)$  and  $d(x)$  for uniform over  $[0, 1]$ .

## 5.2 Limit of Graph Laplacian Regularizer

The following graph Laplacian regularizer is a popular penalty term in many semi-supervised learning algorithms when  $\alpha = 0$ .

$$f^T L_{\alpha, t, n}^u f = \frac{1}{2} \sum_{i, j=1}^n \frac{K_t(X_i, X_j)}{[d_{\alpha, t}(X_i) d_{\alpha, t}(X_j)]^\alpha} (f(X_i) - f(X_j))^2 \quad (39)$$

This limit is studied in (Hein, 2005, Chapter 2) without considering the boundary, and is also studied on  $\mathbb{R}^N$  by (Bosquet et al., 2004), which has no boundary and is not a low dimensional manifold either. From Theorem (2), we see that the graph Laplacian has a limit of different scaling behavior on the boundary points compared to the interior points. This leads to the question of the limit of the graph Laplacian regularizer  $f^T L_{\alpha, t, n}^u f$  when it is defined on a compact submanifold with a smooth boundary. Based on the quadratic form, we use a similar method as the proof of Theorem (2) to obtain the next theorem.

**Theorem 3** For a fixed function  $f(x) \in C^1(\bar{\Omega})$ , and let  $p(x) \in C^\infty(\bar{\Omega})$ ,  $0 < a \leq p(x) \leq b < \infty$ , and the intrinsic dimension of  $\bar{\Omega}$  be  $d$ , then as  $n \rightarrow \infty$ ,  $t \rightarrow 0$  and  $n^2 t^{d+2} \rightarrow \infty$ ,

$$\lim_{n \rightarrow \infty} \frac{1}{n^2 t} f^T L_{\alpha, t, n}^u f = C \int_{\bar{\Omega}} \|\nabla f(x)\|^2 [p(x)]^{2-2\alpha} dx, \quad \text{in probability} \quad (40)$$

where  $C = \frac{1}{4} \pi^{d(1/2-\alpha)}$ .

**Proof:** Following the proof of Theorem (2), let  $\Omega_1$  be a thin lay of “shell” of width  $O(\sqrt{t})$ , and  $\Omega_0 = \bar{\Omega}/\Omega_1$ . For a fixed  $t$ , consider the quadratic form (39), the limit as  $n \rightarrow \infty$  is

$$\frac{1}{2} \iint_{\bar{\Omega}} \frac{K_t(x, y)}{d_t^\alpha(x) d_t^\alpha(y)} (f(x) - f(y))^2 p(y) p(x) dy dx \quad (41)$$

Then by the approximation on manifolds (25) and (26), for a fixed  $x \in \overline{\Omega}$ ,

$$\begin{aligned}
& \frac{1}{2t^{d/2}} p(x) d_t^{-\alpha}(x) \int_{\overline{\Omega}} K\left(\frac{\|x-y\|^2}{t}\right) d_t^{-\alpha}(y) (f(x) - f(y))^2 p(y) dy \\
&= \frac{1}{2t^{d/2}} p(x) d_t^{-\alpha}(x) \int_{\mathbb{T}(x)} K\left(\frac{\|u\|^2}{t}\right) d_t^{-\alpha}(x) (u^T \nabla f(x))^2 p(x) du + O(t^{3/2}) \\
&= \frac{1}{2t^{d/2}} p^2(x) d_t^{-2\alpha}(x) \|\nabla f(x)\|^2 \int_{\mathbb{T}(x)} K\left(\frac{\|u\|^2}{t}\right) u_1^2 du + O(t^{3/2}) \\
&= \frac{t}{2} p^2(x) d_t^{-2\alpha}(x) \|\nabla f(x)\|^2 \int_{\mathbb{T}(x)} K(\|u\|^2) u_1^2 du + O(t^{3/2})
\end{aligned} \tag{42}$$

Notice that in this case, the highest order is controlled by  $(f(x) - f(y))^2$ , which is of order  $O(t)$ , and  $\mathbb{T}(x)$  is the tangent space at  $x$ . Then for any point  $x \in \overline{\Omega}$ , the limit is

$$\frac{C_2(x)}{2C_1^{2\alpha}(x)} \|\nabla f(x)\|^2 [p(x)]^{2-2\alpha} \tag{43}$$

where

$$C_2(x) = \int_{-\infty}^{+\infty} \dots \int_{-\infty}^{+\infty} \int_{-z}^{+\infty} e^{-\|u\|^2} u_1^2 du \tag{44}$$

$$C_1(x) = \int_{-\infty}^{+\infty} \dots \int_{-\infty}^{+\infty} \int_{-z}^{+\infty} e^{-\|u\|^2} du$$

with  $z$  as the distance between  $x$  and the nearest boundary point along the normal direction.

On  $\Omega_0$ , for a small  $t$ , we can replace  $z$  with  $\infty$ , then the integral on  $\Omega_0$  is

$$\frac{C_2}{2C_1^{2\alpha}} \int_{\Omega_0} \|\nabla f(x)\|^2 [p(x)]^{2-2\alpha} dx \tag{45}$$

where the coefficient becomes a constant independent of  $x$ .

On the shell  $\Omega_1$ , as  $t \rightarrow 0$ , the shell shrinks into a set with measure zero. As long as the function inside the integral is bounded, the integral on  $\Omega_1$  will also be zero. For  $x \in \Omega_1$ , we have  $0 \leq z < +\infty$  and

$$\frac{1}{8} \pi^{d/2} \leq C_2(x) = \frac{1}{4} \pi^{d/2} \left(1 - \frac{2z}{\sqrt{\pi e^{z^2}}} + \operatorname{erf}(z)\right) \leq \pi^{d/2} \tag{46}$$

$$\frac{1}{2} \pi^{d/2} \leq C_1(x) = \frac{1}{2} \pi^{d/2} (1 + \operatorname{erf}(z)) \leq \pi^{d/2}$$

For  $f \in C^1(\overline{\Omega})$  and any  $x \in \overline{\Omega}$ , in any direction,  $|\frac{\partial f(x)}{\partial x_i}| < \infty$ . The density  $p(x)$  is also bounded, therefore, the integral on  $\Omega_1$  is zero as  $t \rightarrow 0$ . Overall, as  $t \rightarrow 0$ ,  $C_2(x) \rightarrow C_2$ ,  $C_1(x) \rightarrow C_1$ , and  $\Omega_0$  becomes  $\overline{\Omega}$ , therefore,

$$\lim_{t \rightarrow 0} \frac{1}{2t} \iint_{\overline{\Omega}} \frac{K_t(x, y)}{d_t^\alpha(x) d_t^\alpha(y)} (f(x) - f(y))^2 p(y) p(x) dy dx = \frac{C_2}{2C_1^{2\alpha}} \int_{\overline{\Omega}} \|\nabla f(x)\|^2 [p(x)]^{2-2\alpha} dx \tag{47}$$

Next consider

$$\frac{1}{n^2 t} f^T L_{\alpha, t, n}^u f = \frac{1}{2n^2 t} \sum_{i, j} K_t(X_i, X_j) [d_{\alpha, t, n}(X_i) d_{\alpha, t, n}(X_j)]^{-\alpha} [f(X_i) - f(X_j)]^2 \tag{48}$$

Since all the  $n^2$  terms in the sum are not i.i.d., we use the McDiarmid's inequality. The maximum change of replacing one random variable is

$$\frac{1}{2n^2 t^{d/2+1}} \cdot a^{-2\alpha} \cdot (2M)^2 \tag{49}$$

therefore,

$$P\left(\left|\frac{1}{n^2 t} f^T L_{\alpha, t, n}^u f - C \int_{\overline{\Omega}} \|\nabla f(x)\|^2 [p(x)]^{2-2\alpha} dx\right| > \epsilon\right) \leq 2e^{-\frac{n^2 t^{d/2+1} \epsilon^2 a^{4\alpha}}{2M^4}} \tag{50}$$

We conclude the proof by plugging in  $C_1 = \pi^{d/2}$  and  $C_2 = \frac{1}{2} \pi^{d/2}$ . ■

One important implication of this theorem is that, in order to use a gradient penalty term w.r.t. to different density weights in the form of  $p^s(x)$  in the limit, we can use  $f^T L_{\alpha, t, n}^u f$  with different  $\alpha$  values. For instance, to obtain  $\int_{\overline{\Omega}} \|\nabla f(x)\|^2 p(x) dx$  instead of having  $p^2(x)$  as the commonly used penalty term  $f^T L^u f$ , we can set  $\alpha = 1/2$ . This penalty then fits the fact that sample  $X_i$  are drawn from density  $p(x)$ .

We tested Theorem (3) numerically on several functions with a uniform density over 1-dimensional interval  $[0, 1]$ . 1001 equal-space points are generated, the value of  $t$  is between 1 and  $10^{-7}$ , and we compute

Table 2: Coefficient test for different functions. The largest value for different  $t$  of each function is reported.

$\alpha \backslash f(x)$	$\sqrt{x+1}$	$x$	$x^2 + 10x$	$x^3$	$e^x$	$\sin(x)$	$\cos(x)$	$\cos(10x)$	$\frac{1}{4}\pi^{(1/2-\alpha)}$
0	0.4424	0.4424	0.4424	0.4420	0.4423	0.4424	0.4423	0.4426	0.4431
1/2	0.2497	0.2497	0.2497	0.2497	0.2497	0.2497	0.2497	0.2497	0.2500
1	0.1411	0.1411	0.1411	0.1412	0.1411	0.1412	0.1410	0.1411	0.1410
-1	1.3845	1.3846	1.3846	1.3819	1.3840	1.3827	1.3865	1.3859	1.3921

the numerical graph Laplacian approximation  $\frac{1}{n^{2t}} f^T L_{\alpha,t,n}^u f$ , and the analytical value of  $\int_0^1 |f'(x)|^2 dx$ . The ratios of the two are reported in Table (2) and the coefficient plots as a function of  $\log(t)$  are shown in Figure (7).

In Figure (7), eight different functions from Table (2) are tested for the coefficient  $C$  using different bandwidth  $t$ . Each plot corresponds to one fixed  $\alpha$  value. As suggested by the figure, in Table (2), the maximum values from different  $t$  are reported. From both the figure and the table we can see that, the numerical results are close to the theoretical coefficient  $\frac{1}{4}\pi^{1/2-\alpha}$ . The figure also suggests a numerically stable patterns as  $t$  decreases, until it is too small and loses numerical precision.

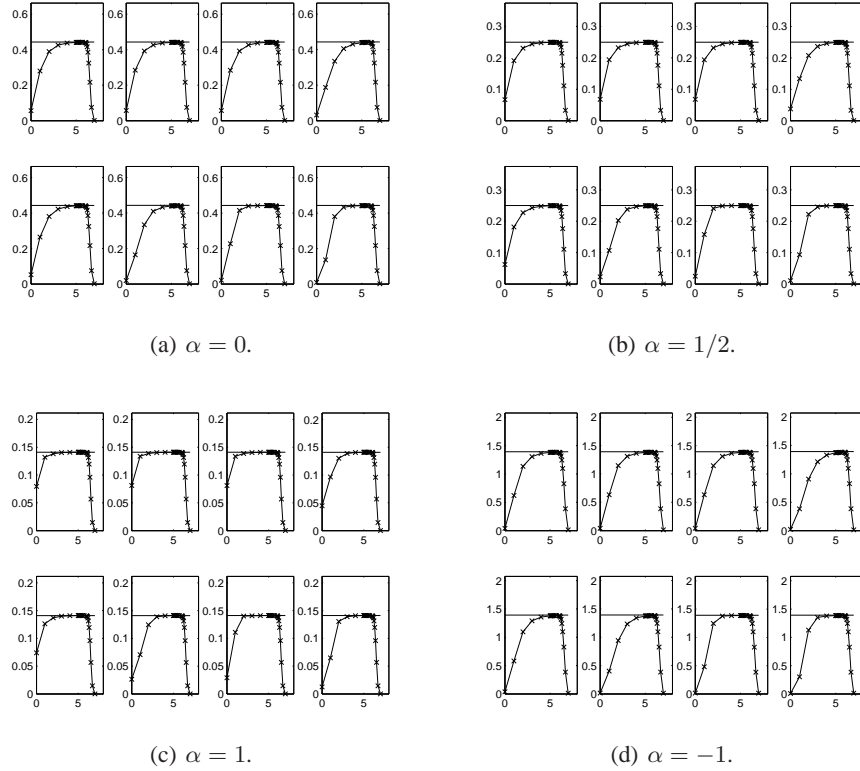


Figure 7: Coefficient  $C$  as a function of  $t$  for different functions. The solid line is the theoretical result, and the  $x$  axis corresponds to  $-\log(t)$ .

Notice that on finite samples, it is also possible to treat  $f^T L_{\alpha,t,n}^u f$  as an inner product as  $\langle f, L_{\alpha,t,n}^u f \rangle$ . However, in the limit, as we see in this paper,  $L_{\alpha,t,n}^u f$  can degenerate to an unbounded value on the boundary. Although this behavior only happens on a small part having volume  $O(t^{1/2})$  and the degenerating behavior scales as  $t^{1/2}$ , they cannot cancel out each other since we can not bring the limit  $t \rightarrow 0$  across the integral when the sequence of functions inside of the integral have an unbounded limit, i.e., it violates the condition of Dominated Convergence Theorem. When  $f$  satisfy the Neumann boundary condition or  $\bar{\Omega}$  has no boundary,

then it is safe to compute the limit as an inner product, which is essentially the Green's first identity.

### 5.3 Reproducing Kernels and Boundary Effects

In the short discussion below we would like to illustrate the importance of boundary effects in a simple 1-dimensional setting. Consider the regularizer  $f^T L^u f$ , whose limit for a fixed  $f$  in  $\mathbb{R}^N$  has the following expression (Bosquet et al., 2004).

$$J(f) = \int_{\mathbb{R}^N} \|\nabla f(x)\|^2 p^2(x) dx$$

In  $\mathbb{R}^1$ , the subspace orthogonal to the null space of  $J(f)$  is a reproducing kernel Hilbert space (RKHS) (Nadler et al., 2009).

Consider its reproducing kernel function  $K(x, y)$ . Over the unit interval  $[0, 1]$  with uniform probability density the kernel function can be found explicitly by eigenfunction expansion of the Green's function of the weighted Laplacian (Green's function in this case is the same as kernel  $K(x, y)$ ). Using the Neumann boundary condition, we find that the reproducing kernel (in the subspace orthogonal to the null space) has the following expression:

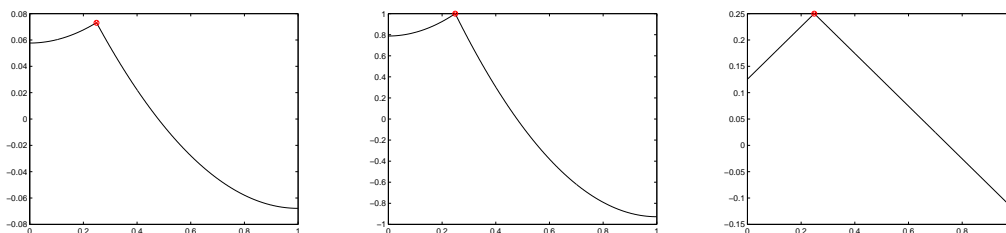
$$K(x, y) = \sum_{k=1}^{\infty} \frac{1}{(k\pi)^2} \cos(k\pi x) \cos(k\pi y) \quad (51)$$

On the other hand, in (Nadler et al., 2009) the kernel without boundary conditions is shown to be

$$K'(x, y) = \frac{1}{4} - \frac{1}{2}|x - y| \quad (52)$$

which is a different function.

In order to test our analysis, we notice that in finite sample case the discrete Green's function of  $L_{\alpha, t, n}^u$  is the same as the reproducing kernel functions for space  $\{f : f^T L_{\alpha, t, n}^u f < \infty\}$ , which is the pseudoinverse of the matrix  $L_{\alpha, t, n}^u$  (Berlinet & Thomas-Agnan, 2003, Chapter 6). In Figure (8), we compute and plot the kernels numerically to verify the above analysis. On one hand, we use the eigenfunction expansion (51) to find the kernel. On the other hand, we build the graph Laplacian matrix and compute its pseudoinverse to obtain the approximate kernel function. As shown in Figure (8), we can see that the kernel obtained by eigenfunction expansion analytically is very close to the one obtained from the pseudoinverse of the matrix  $L_{\alpha, t, n}^u$  (up to a constant scaling factor). This kernel is quite different from  $K'$ . The difference is due to the global effect of the boundary behavior of the graph Laplacian and provides additional evidence for the Neumann boundary condition in eigenfunctions.



(a) Kernel  $K$  by eigenfunction expansion (b) Kernel  $K$  by pseudoinverse of the graph Laplacian

(c) Kernel  $K'$

Figure 8: Kernels at 0.25 over  $[0, 1]$  in subspace that is orthogonal to the null of  $L_{\alpha, t, n}^u$ .

## References

- Allaire, G. (2007). *Numerical analysis and optimization : an introduction to mathematical modelling and numerical simulation*. Oxford University Press, 2007.
- Belkin, M. (2003). *Problems of learning on manifold*. Doctoral dissertation, University of Chicago.
- Belkin, M., & Niyogi, P. (2003). Laplacian eigenmaps for dimensionality reduction and data representation. *Neural Comp*, 15, 1373–1396.

- Belkin, M., & Niyogi, P. (2007). Convergence of Laplacian Eigenmaps. In B. Schölkopf, J. Platt and T. Hoffman (Eds.), *Advances in neural information processing systems 19*, 129–136. Cambridge, MA: MIT Press.
- Belkin, M., & Niyogi, P. (2008). Towards a Theoretical Foundation for Laplacian-Based Manifold Methods. *Journal of Computer and System Sciences*, 74, 1289–1308.
- Berlinet, A., & Thomas-Agnan, C. (2003). *Reproducing Kernel Hilbert Spaces in Probability and Statistics*. Kluwer Academic Publishers.
- Bosquet, O., Chapelle, O., & Hein, M. (2004). Measure Based Regularization. *Advances in Neural Information Processing Systems 16*.
- Chapelle, O., Schölkopf, B., & Zien, A. (2006). *Semi-supervised Learning*. MIT Press.
- Coifman, R. R., & Lafon, S. (2006). Diffusion maps. *Applied and Computational Harmonic Analysis*, 21, 5–30.
- Giné, E., & Koltchinskii, V. (2006). Empirical Graph Laplacian Approximation of Laplace-Beltrami Operators: Large Sample Results. 51, 238–259.
- Hein, M. (2005). *Geometrical aspects of statistical learning theory*. Doctoral dissertation, Wissenschaftlicher Mitarbeiter am Max-Planck-Institut für biologische Kybernetik in Tübingen in der Abteilung.
- Hein, M., Yves Audibert, J., & Luxburg, U. V. (2007). Graph Laplacians and their Convergence on Random Neighborhood Graphs. *Journal of Machine Learning Research*, 8, 1325–1368.
- Lafon, S. (2004). *Diffusion Maps and Geodesic Harmonics*. Doctoral dissertation, Yale University.
- Maier, M., Hein, M., & von Luxburg, U. (2009). Optimal construction of k-nearest-neighbor graphs for identifying noisy clusters. *Theoretical Computer Science*, 410, 1749–1764.
- Nadler, B., Srebro, N., & Zhou, X. (2009). Semi-Supervised Learning with the Graph Laplacian: The Limit of Infinite Unlabelled Data. *Twenty-Third Annual Conference on Neural Information Processing Systems*.
- Rosasco, L., M. Belkin, & Vito, E. D. (2010). On Learning with Integral Operators. *Journal of Machine Learning Research*, 11, 905–934.
- Singer, A. (2006). From graph to manifold Laplacian: The convergence rate. *Appl. Comput. Harmon. Anal.*, 21, 128–134.
- von Luxburg, U. (2007). A Tutorial on Spectral Clustering. *Statistics and Computing* (pp. 395–416).
- von Luxburg, U., Belkin, M., & Bousquet, O. (2008). Consistency of spectral clustering. *Ann. Statist.*, 36, 555–586.
- Zhou, X., & Belkin, M. (2011). Semi-supervised Learning by Higher Order Regularization. *The 14th International Conference on Artificial Intelligence and Statistics*.
- Zhu, X. (2006). Semi-supervised learning literature survey. *Computer Science, University of Wisconsin-Madison*.
- Zhu, X., Lafferty, J., & Ghahramani, Z. (2003). Semi-Supervised Learning Using Gaussian Fields and Harmonic Function. *The Twentieth International Conference on Machine Learning*.